AIP Applied Physics Letters

A simple design of flat hyperlens for lithography and imaging with half-pitch resolution down to 20 nm

Yi Xiong, Zhaowei Liu, and Xiang Zhang

Citation: Applied Physics Letters **94**, 203108 (2009); doi: 10.1063/1.3141457
View online: http://dx.doi.org/10.1063/1.3141457
View Table of Contents: http://scitation.aip.org/content/aip/journal/apl/94/20?ver=pdfcov
Published by the AIP Publishing

Articles you may be interested in
Enhancing aspect profile of half-pitch 32 nm and 22 nm lithography with plasmonic cavity lens
Appl. Phys. Lett. **106**, 093110 (2015); 10.1063/1.4914000

Optimizing photon sieves to approach Fresnel diffraction limit via pixel-based inverse lithography
J. Vac. Sci. Technol. B **29**, 041002 (2011); 10.1116/1.3605473

Fabrication of half-pitch 32 nm resist patterns using near-field lithography with a - Si mask
Appl. Phys. Lett. **89**, 033113 (2006); 10.1063/1.2227633

Submicron imaging with a planar silver lens
Appl. Phys. Lett. **84**, 4403 (2004); 10.1063/1.1757644

Design and characterization of a high numerical aperture lens system for scanned laser lithography
J. Vac. Sci. Technol. B **15**, 2193 (1997); 10.1116/1.589612

This article is copyrighted as indicated in the article. Reuse of AIP content is subject to the terms at: http://scitation.aip.org/termsconditions. Downloaded to IP: 136.152.209.32 On: Mon, 29 Jun 2015 17:35:28

A simple design of flat hyperlens for lithography and imaging with half-pitch resolution down to 20 nm

Yi Xiong,[1] Zhaowei Liu,[1,a)] and Xiang Zhang[1,2,b)]
[1]*NSF Nanoscale Science and Engineering Center (NSEC), University of California, Berkeley, California 94720, USA*
[2]*Materials Sciences Division, Lawrence Berkeley National Laboratory, 1 Cyclotron Road, Berkeley, California 94720, USA*

(Received 14 March 2009; accepted 3 May 2009; published online 20 May 2009)

We propose that a hyperlens can be used for photolithography to generate deep subwavelength arbitrary patterns from diffraction-limited masks. Numerical simulation shows that half-pitch resolution down to 20 nm is possible from a mask with 280 nm period at working wavelength 375 nm. We also extend the hyperlens projection concept from cylindrical interfaces to arbitrary interfaces. An example of a flat interface hyperlens is numerically demonstrated for lithography purposes. © *2009 American Institute of Physics*. [DOI: 10.1063/1.3141457]

The rapid progress in nanoscale science and technology requires maintaining the fast pace of reducing the pitch resolution of photolithography. Conventional photolithography keeps reducing the illumination wavelength to keep up with the resolution demand. However, as the illumination wavelength moves from UV to deep UV and extreme UV, the instrument complexity and cost increase dramatically. Alternatively, it has been demonstrated that plasmonic lithography[1–10] can work at conventional UV wavelength yet achieve higher resolution by breaking the diffraction limit of light. Plasmonic lithography utilizes surface plasmon polaritons.[11,12] The wavelength of surface plasmon polaritons is much smaller than that of light that excites them, which enables high-resolution photolithography.

Recently, a subdiffraction-limited imaging device called hyperlens attracted significant attention.[13–19] A hyperlens is composed of a curved periodic stack of metal-dielectric multilayers. The hyperlens breaks the diffraction limit by magnifying the subdiffraction-limited objects and projecting the magnified images to the far field. Based on reciprocity theorem, a hyperlens can also be used for subdiffraction-limited photolithography, which can generate subdiffraction-limited arbitrary patterns either from diffraction-limited masks or interference patterns of illumination light. In other words, it can be either a mask or a maskless photolithography scheme.

The hyperlens in Ref. 17 has cylindrical surfaces. It is more desirable if a photolithography scheme has the flexibility to generate patterns on arbitrarily shaped surfaces. In Ref. 20, it is reported that compressible silicon can implement electronic or optoelectronic system on nonplanar surfaces, though the feature sizes of the patterns are in micron scale. A hyperlens can be designed in a way that subdiffraction-limited arbitrary patterns are generated at arbitrarily shaped surfaces. Figure 1 shows an example to realize such a design [Fig. 1(b)] from our original hyperlens configuration [Fig. 1(a)]. The input and output surfaces of the hyperlens are polished into arbitrary shapes as desired. Specifically, it is of great interest to generate arbitrary patterns with subdiffraction-limited features on flat surfaces. It is worth mentioning that another generation of hyperlens with flat surfaces[21–23] was proposed recently. That type of hyperlens is made of a metamaterial with complex distribution of refractive index where light is manipulated to propagate along designed paths at arbitrary scales. It is quite challenging, despite the elegant concept, to realize such a hyperlens considering current fabrication abilities. In this paper, we use numerical simulations to demonstrate a feasible design that subdiffraction-limited patterns can be generated from diffraction-limited masks by the original hyperlens with flat input and output surfaces, as shown in Fig. 1(c).

The principle of hyperlens imaging and lithography can be explained by using dispersion relation of electromagnetic waves in cylindrical coordinates: $k_r^2/\varepsilon_\theta + k_\theta^2/\varepsilon_r = k_0^2$, where k_r and k_θ are wave vectors, ε_r and ε_θ are the permittivities of the medium in radial and tangential directions, respectively, and k_0 is the wave vector in free space ($k_0 = 2\pi/\lambda$, where λ is the free space wavelength). In an isotropic medium $\varepsilon_r = \varepsilon_\theta = \varepsilon$, waves with tangential wave vector k_θ larger than $\sqrt{\varepsilon} k_0$, called evanescent waves, decay exponentially. A hyperlens is designed to be an effective anisotropic medium with negative

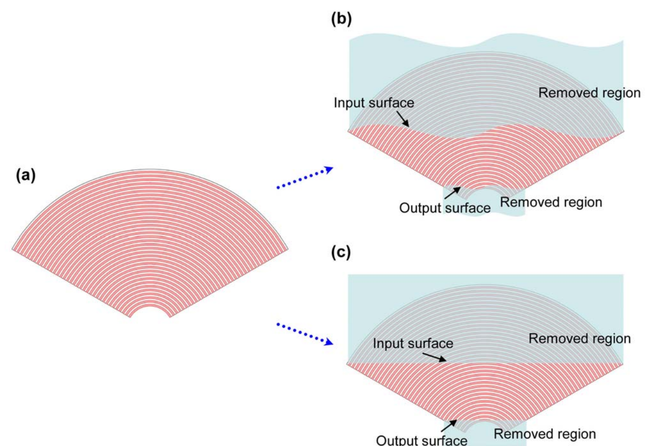

FIG. 1. (Color online) Schematics of extending the original hyperlens into various geometries. (a) The original hyperlens, (b) a hyperlens with arbitrary input and output surfaces, and (c) a hyperlens with flat input and output surfaces.

[a)]Present address: Department of ECE, University of California, San Diego, La Jolla, California 92093, USA.
[b)]Author to whom correspondence should be addressed. Electronic addresses: xiang@berkeley.edu and xzhang@me.berkeley.edu.

 © 2009 American Institute of Physics

This article is copyrighted as indicated in the article. Reuse of AIP content is subject to the terms at: http://scitation.aip.org/termsconditions. Downloaded to IP: 136.152.209.32 On: Mon, 29 Jun 2015 17:35:28

ε_r and positive ε_θ so that waves with arbitrarily large tangential wave vector k_θ can propagate in the hyperlens. For imaging purposes, the object with subdiffraction-limited features is placed near the inner surface of a hyperlens. Waves with arbitrarily large tangential wave vector k_θ corresponding to subdiffraction-limited features can propagate through the hyperlens. In addition, the tangential wave vectors are gradually compressed as the waves propagate outward along the radial direction due to the cylindrical geometry of the hyperlens. Consequently, the subdiffraction-limited features can be magnified by the hyperlens and then captured by conventional optics to form an image with subdiffraction-limited resolution. For lithography purposes, the diffraction-limited pattern is projected onto the outer surface of a hyperlens from a diffraction-limited mask. As the waves propagate inward along the radial direction, tangential wave vectors are gradually increased while the waves can still propagate in the hyperlens. As a result, a diffraction-limited pattern of the mask can be reduced to a subdiffraction-limited pattern at the inner surface of the hyperlens.

The working wavelength of the hyperlens made of Ag and Al_2O_3 in Ref. 17 is 365 nm. In this paper, the hyperlens is still composed of Ag and Al_2O_3 cylindrical multilayers but works at wavelength 375 nm. At wavelength 375 nm [the permittivities $\varepsilon_{Ag}=-3.12+0.21i$ (Ref. 24) and $\varepsilon_{Al_2O_3}=3.21$ (Ref. 25)], the dispersion relation of electromagnetic waves in the hyperlens has smaller hyperbolic curvature (flatter) than that at 365 nm wavelength. The hyperlens with flatter hyperbolic dispersion relation is ideal to achieve high resolution for optical imaging or lithography because the change in k_r can be minimized as k_θ varies, which prevents phase mismatch between waves with different k_θ.

We first use a simulation to demonstrate that a cylindrical hyperlens can generate one-dimensional (1D) subdiffraction-limited patterns from diffraction-limited masks. In Fig. 2(a), the hyperlens is made of 10 nm Ag and 10 nm Al_2O_3 cylindrical multilayers. The inner and outer radius of the hyperlens is 120 and 790 nm. The Cr mask [at 375 nm wavelength $\varepsilon_{Cr}=-8.98+9.36i$ (Ref. 26)] with thickness 50 nm on the outer surface of the hyperlens has periodic openings with 280 nm period and 140 nm width. The polarization is TM polarization, and the H field is defined to be 1 at the openings along the input surface, as shown in Fig. 2(b). The reduction factor is determined by the radius ratio of input and output surfaces, which is $840/120=7$. Photoresist with permittivity 2.89 (negative photoresist NFR 105G from JSR Micro) is placed inside the output surface. The simulation carried out by COMSOL MULTIPHYSICS 3.4 shows that at the output surface, a pattern with 40 nm period is formed, which is expected as the reduction time of the hyperlens is 7. Figure 2(c) shows the $|E|$ field along the output surface. The intensity contrast is $(|E|^2_{max}-|E|^2_{min})/(|E|^2_{max}+|E|^2_{min})\approx 0.33$,

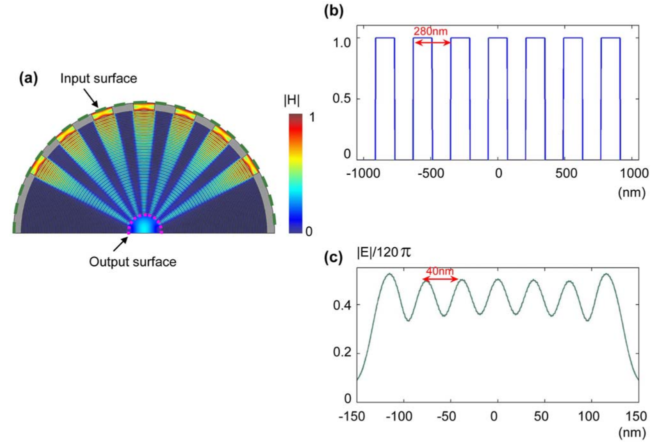

FIG. 2. (Color online) Generating 1D subdiffraction-limited patterns from a diffraction-limited mask by a cylindrical hyperlens. (a) $|H|$ field distribution in the hyperlens. (b) H field along the input surface. The period of the openings is 280 nm. (c) $|E|$ field distribution along the output surface.

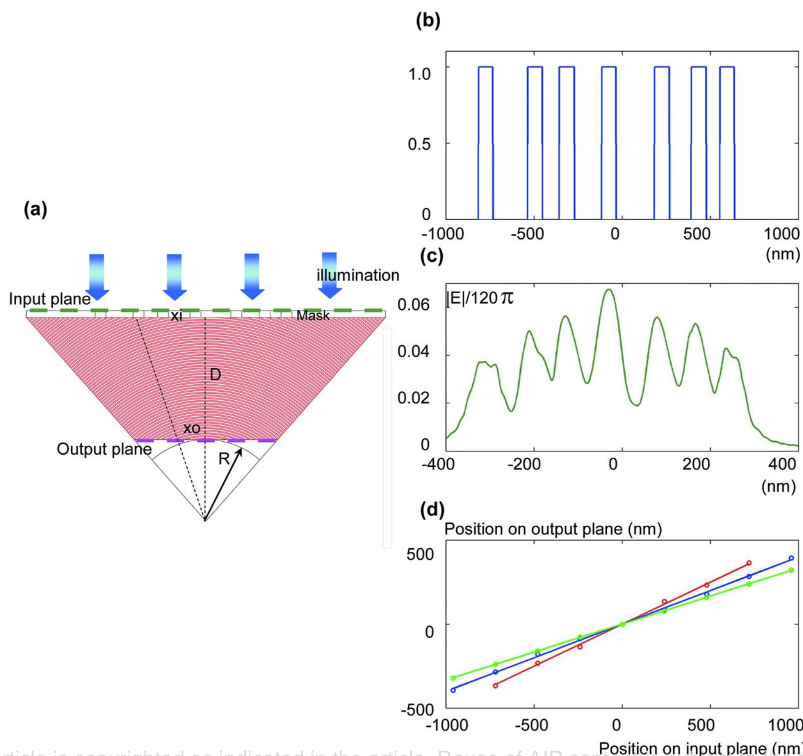

FIG. 3. (Color online) (a) A schematic of a flat interface hyperlens. (b) At the input plane, H field is defined to be 1 at the seven openings with 80 nm width on the mask. TM polarization is used in the simulation. From left to right, the distances between the openings are 280, 180, 240, 300, 210, and 160 nm. (c) $|E|$ field distribution along the plane that is 10 nm below the output plane. From left to right, the distances between peaks are 101, 82, 100, 108, 87, and 70 nm. (d) Reduction characteristics of the flat interface hyperlens. The lines are linear reduction relations calculated by the formula. The reduction factors are two times for red line ($D=600$ nm, $R=600$ nm), 2.5 times for blue line ($D=900$ nm, $R=600$ nm), and three times for green line ($D=1200$ nm, $R=600$ nm). The dots are simulation data.

This article is copyrighted as indicated in the article. Reuse of AIP content is subject to the terms at: http://scitation.aip.org/termsconditions. Downloaded to IP: 136.152.209.32 On: Mon, 29 Jun 2015 17:35:28

which is larger than the minimum contrasts required for common negative photo resists.

We can polish the hyperlens to obtain flat input and output planes as shown in Fig. 3(a). Linear reduction characteristics can be defined in such a flat interface hyperlens by an exact formula

$$xi/xo = (R + D)/R,$$

where R is the radius of the inner surface of the original hyperlens, and D is the thickness of the flat hyperlens.

According to the above equation, the hyperlens in Fig. 3(a) ($D=900$ nm and $R=600$ nm) demagnifies the 1D arbitrary pattern by 2.5 times. Seven openings distribute arbitrarily at the input plane [Fig. 3(b)]. The generated pattern at the output plane [Fig. 3(c)] is the demagnified pattern at the input plane with a reduction factor of about 2.5, which agrees with the reduction factor formula. The $|E|$ field is stronger at the center than at the side because the flat hyperlens has less pairs of metal-dielectric layers at the center.

The hyperlens in Fig. 3(a) is only one example. The same principle can be applied to various designs with different reduction factors. Figure 3(d) shows the reduction characteristics of the flat interface hyperlens. The configuration of the hyperlens is similar to that in Fig. 3(a). The lines are linear reduction relations calculated by the above formula. The dots are simulation data. The maximum variation between the simulation data and formula expectation is 16 nm. The variation is the result of the finite thickness of the metal and dielectric layers. The simulation results show design flexibility of the flat interface hyperlens, which can have various reduction factors. The results also verify its linear reduction characteristics.

Ideally, the resolution of the hyperlens has no limit as the reduction factor of the hyperlens is determined by the geometrical parameters of the hyperlens. Practically, however, the material loss and the fabrication abilities limit the resolution. Currently, the best half-pitch resolution of a flat interface hyperlens in our simulations is 20 nm (not shown here). Smaller half-pitch size is possible if the thickness of the metal and dielectric layers is reduced. The working wavelength can be changed to wavelengths other than 375 nm by selecting other materials. For example, a hyperlens made of Al and SiO_2 multilayers can work at wavelength 157 nm. It is also worthy to mention that spherical metal-dielectric multilayers can be used if a two-dimensional subdiffraction-limited arbitrary pattern is desired.

In conclusion, we propose a scheme to use a hyperlens to project subdiffraction-limited patterns on arbitrarily shaped surfaces from diffraction-limited masks. Specifically, we numerically verify that a hyperlens with flat input and output planes can generate subdiffraction-limited arbitrary patterns. The simulation results show that the patterns generated at the flat output plane of the hyperlens is the linear reduction of the patterns at the flat input plane.

The authors thank Dr. Guy Bartal for valuable discussions. This work was supported by the U.S. Department of Energy under Contract No. DE-AC02-05CH11231 and the National Science Foundation (NSF) Nanoscale Science and Engineering Center (Grant No. CMMI-0751621).

[1] R. J. Blaikie and S. J. McNab, Appl. Opt. **40**, 1692 (2001).
[2] J. G. Goodberlet and H. Kavak, Appl. Phys. Lett. **81**, 1315 (2002).
[3] W. Srituravanich, N. Fang, C. Sun, Q. Luo, and X. Zhang, Nano Lett. **4**, 1085 (2004).
[4] X. Luo and T. Ishihara, Opt. Express **12**, 3055 (2004).
[5] D. O. S. Melville and R. J. Blaikie, J. Vac. Sci. Technol. B **22**, 3470 (2004).
[6] Z. W. Liu, Q. H. Wei, and X. Zhang, Nano Lett. **5**, 957 (2005).
[7] D. B. Shao and S. C. Chen, Appl. Phys. Lett. **86**, 253107 (2005).
[8] T. Xu, Y. Zhao, J. Ma, C. Wang, J. Cui, C. Du, and X. Luo, Opt. Express **16**, 13579 (2008).
[9] Y. Xiong, Z. W. Liu, and X. Zhang, Appl. Phys. Lett. **93**, 111116 (2008).
[10] Y. Xiong, Z. W. Liu, and X. Zhang, U.S. Provisional application was filed. See disclosure at http://ipira.berkeley.edu/inventiondetail.php?inventionId=1001849.
[11] R. H. Ritchie, Phys. Rev. **106**, 874 (1957).
[12] W. L. Barnes, A. Dereux, and T. W. Ebbesen, Nature (London) **424**, 824 (2003).
[13] Z. Jacob, L. V. Alekseyev, and E. Narimanov, Opt. Express **14**, 8247 (2006).
[14] A. Salandrino and N. Engheta, Phys. Rev. B **74**, 075103 (2006).
[15] N. Fang, H. Lee, C. Sun, and X. Zhang, Science **308**, 534 (2005).
[16] V. A. Podolskiy and E. E. Narimanov, Opt. Lett. **30**, 75 (2005).
[17] Z. W. Liu, H. Lee, Y. Xiong, C. Sun, and X. Zhang, Science **315**, 1686 (2007).
[18] H. Lee, Z. W. Liu, Y. Xiong, C. Sun, and X. Zhang, Opt. Express **15**, 15886 (2007).
[19] A. V. Kildishev and E. E. Narimanov, Opt. Lett. **32**, 3432 (2007).
[20] H. C. Ko, M. P. Stoykovich, J. Song, V. Malyarchuk, W. M. Choi, C. J. Yu, J. B. Geddes III, J. Xiao, S. Wang, Y. Huang, and J. A. Rogers, Nature (London) **454**, 748 (2008).
[21] A. V. Kildishev and V. M. Shalaev, Opt. Lett. **33**, 43 (2008).
[22] V. M. Shalaev, Science **322**, 384 (2008).
[23] S. Han, Y. Xiong, D. Genov, Z. W. Liu, G. Bartal, and X. Zhang, Nano Lett. **8**, 4243 (2008).
[24] P. B. Johnson and R. W. Christy, Phys. Rev. B **6**, 4370 (1972).
[25] M. J. Weber, *Handbook of Optical Materials* (CRC, Boca Raton, 2003).
[26] D. R. Lide, *Handbook of Chemistry and Physics* (CRC, Boca Raton, 2001).

This article is copyrighted as indicated in the article. Reuse of AIP content is subject to the terms at: http://scitation.aip.org/termsconditions. Downloaded to IP: 136.152.209.32 On: Mon, 29 Jun 2015 17:35:28